ELSEVIER

Materials Science and Engineering A203 (1995) 134–139

MATERIALS SCIENCE & ENGINEERING A



# Influence of solidification on the microstructural evolution of nickel base weld metal

J.S. Ogborn[a], D.L. Olson[a], M.J. Cieslak[b]

[a]*Department of Metallurgical and Materials Engineering, Center for Welding and Joining Research, Colorado School of Mines, Golden, CO 80401, USA*

[b]*Sandia National Laboratory, Albuquerque, NM 87185, USA*

Received 3 March 1995

**Abstract**

The effect of segregation resulting from solidification on the microstructural evolution of nickel base alloys was investigated. Two different groups of alloys were produced to simulate either the Hastelloy C type or the Inconel 625/718 type of alloys. Gravitational thermal analysis welding was performed on these experimental alloys and the extent of microsegregation in the weld metal was determined. Using composition profiles obtained from solidified microstructures, predictions of the phase stability of these microstructures were made based on metal d-level ($M_d$) calculations. The maximum $M_d$ values obtained in these microstructures were compared with those critical to the formation of topologically close-packed (TCP) phases such as sigma, P, and Laves. These profiles showed an increase in the $M_d$ level in the interdendritic regions which was correlated to the formation of TCP phases.

*Keywords:* Nickel base alloys; Microsegregation; $M_d$ calculations

## 1. Introduction

Nickel base alloys such as Hastelloy C-4 and C-276 as well as Inconel 625 and 718 were developed to withstand the high-temperature and corrosive environments in gas turbines and chemical plants [1,2]. These commercial alloys do not contain any topologically close-packed (TCP) phases in the mill-annealed condition [2,3]. After welding, TCP phases such as sigma, P, and Laves appear in the weld metal microstructure, either as a result of non-equilibrium solidification or after prolonged exposure to elevated temperatures [4,5]. These phases can adversely affect the mechanical and corrosion properties [5–8]. The appearance of these TCP phases suggests that during the non-equilibrium solidification of arc welding, enough segregation occurs locally to achieve a sufficient thermodynamic driving force to form these transformation products. Since the formation of small amounts of TCP phases during welding can lead to weld metal hot cracking [9–12] and a degradation of mechanical and corrosion properties, it would be desirable to predict the susceptibility to their formation for a given alloy composition [13,14].

An obvious method for the prediction of solidification products would be phase diagrams of the alloy system involved. Nickel base alloys are derived from at least four components; usually five or more components. Since phase diagrams which would be applicable to a given commercial alloy are extremely rare, the phase diagram approach usually is problematic.

To consider the complex alloying of superalloys, systematic methods were developed to determine phase stability. The first of these methods, PHACOMP for PHAse COMPutation, uses electron vacancy numbers to determine phase stability [15–21]. More recently New PHACOMP has been developed which calculates the average energy levels of the electron orbitals [22,23].

As early as 1952, Das et al. [15] found a correlation between the electron vacancy number ($N_v$) [16] and phase stability in Mo–Fe–Co, Mo–Fe–Ni, and Mo–Ni–Co ternary systems. This work was continued by Greenfield and Beck [17,18] who examined the formation of sigma phase in systems containing transition


*SSDI* 0921-5093(95)09832-1

elements. In 1968, Woodyatt et al. [19] published a specific procedure to calculate an average $N_v$ for commercial alloys which took into account the contribution of each element. The algebraic equation to determine the average electron vacancy number of an alloy is given as:

$$N_v = \sum_i (X_i)(N_{vi}) \quad (1)$$

where $X_i$ is the atomic fraction of element $i$ and $N_{vi}$ is the electron hole number for that element. Only the elements that were in solid solution were considered, which required a method to reduce the alloy content of compound-forming elements.

Although the electron vacancy method ignores differences in relative electronegativity and size of the atoms, a correlation was found between having calculated $N_v$ values above the critical $N_v$ value and the occurrence of topologically close-packed phases in many alloy systems [15]. This analytical method was used to define phase boundaries. To further refine this method to make up for discrepancies found for some nickel base alloys where significant amounts of sigma phase form within a predicted safe region or where sigma phase did not form at a composition well within a sigma phase prone region [20], Barrows and Newkirk [21] developed a temperature-dependent critical vacancy number ($N_{vc}$). Here, the algebraic coefficients used to determine the $N_v$ are based on solid solubility data from existing phase diagrams. To determine the susceptibility of an alloy to sigma formation, the average $N_v$ is compared with the $N_{vc}$. If $N_v > N_{vc}$, an alloy would be predicted to be sigma-phase prone. Since this method is an extension of the original PHACOMP method its accuracy is limited to the availability of phase diagrams and the electron vacancy concept from which it was derived.

As an extension of the electron vacancy approach New PHACOMP as described by Morinaga [22,23] is based on a theoretical approach to the solubility problem in alloys containing transition elements. Like PHACOMP, New PHACOMP does not predict which TCP phase forms, only the likelihood of a given composition to contain such phases. To predict the type of phase forming on solidification, ternary phase diagrams closely representing the given alloy are used [23].

In the New PHACOMP model, the parameter $M_d$ is introduced and defined as an average energy level above the Fermi level of "d" orbitals in transition elements. The average energy in the metal d-level ($M_d$) of an alloy is calculated by summing the contribution of each alloying element multiplied by its atomic fraction analogous to $N_v$ calculations.

$$M_d = \sum M_{di} X_i \text{ (in eV)} \quad (2)$$

A critical $M_d$ value is determined by fitting the solid solubility line in phase diagrams by a constant $M_d$ line. By plotting the sigma phase safe boundary at different temperatures for various alloys the following equation was developed [22]:

$$M_{dc} = 6.25 \times 10^{-5} T + 0.834 \text{ (in eV)} \quad (3)$$

where temperature $T$ is in absolute Kelvin. As the average $M_d$ exceeds a critical value, $M_{dc}$, the energy associated with the solid solution becomes favourable for a TCP to form. In theory, the $M_{dc}$ should depend on the type of phase forming [21]; however, sigma phase is chemically and structurally similar [14,21] to other TCP phases and historically their critical values have been expressed by the same value [22,23].

New PHACOMP and its predecessors have traditionally been used to predict the electronic structure of wrought alloys. In weld metal, the composition varies with position, as a result of cellular solidification segregation, and bulk composition calculations are no longer valid. Correlation between the New PHACOMP approach and the formation of TCP phases in the weld metal of Hastelloy C-4, C-22, and C-276 as well as Inconel 625 and 718 has been examined by Cieslak et al. [24]. These alloys in wrought form have previously been proven safe for long term high temperature applications [5–7]. Upon further examination of the weld metal, Cieslak et al. [24] found the weld metal to contain the topologically close-packed phases mu, P, sigma, and Laves. In the same study, differential thermal analysis revealed terminal solidification reactions involving some of these phases. These studies were performed on commercial alloys which contain significant alloying additions of cobalt, manganese, and tungsten, as well as other elements.

## 2. Experimental approach

To examine the effect of various alloying elements on the formation of TCP-like phases, two different series of nickel base alloys were produced. Alloy compositions are listed in Table 1. Series I alloys were produced to examine sigma-type phase formation and compare with the austenite solvus in the Ni–Cr–Mo system by varying the relative amounts of chromium, iron, and molybdenum. Series II alloys were designed to contain Laves-type phases. Variations in chromium, iron, and niobium of Series II alloys will alter the electronic structure of the alloy and thus its propensity to form Laves phases.

Small slabs $120 \times 40 \times 3$ mm$^3$ were prepared from each alloy by melting a blend of metallic powders in a vacuum furnace. These slabs were cold rolled to ten-percent reduction, annealed, reduced an additional ten percent, and annealed again. This procedure was per-

Table 1
Composition of experimental alloys as determined by scanning electron microscopy

| Alloy number | Composition (wt.%) | | | | |
|---|---|---|---|---|---|
| | Ni | Cr | Fe | Mo | Nb |
| *Series I* | | | | | |
| 1 | 63.7 | 20.1 | — | 16.2 | — |
| 2 | 51.9 | 17.0 | 15.4 | 15.7 | — |
| 3 | 57.5 | 16.6 | 10.0 | 15.9 | — |
| 4 | 51.7 | 21.9 | 10.0 | 16.4 | — |
| *Series II* | | | | | |
| 5 | 53.0 | 21.9 | 19.9 | — | 5.2 |
| 6 | 62.7 | 21.3 | 10.1 | — | 5.9 |
| 7 | 62.1 | 11.3 | 20.7 | — | 5.9 |
| 8 | 73.8 | 10.3 | 10.4 | — | 5.5 |

formed to homogenize the microstructure prior to welding and to dissolve any phases which may have formed during the initial solidification.

Autogenous gravitational thermal analysis (GTA) welding using argon shielding was performed on each of the eight slabs. Welds were made at 100 A, 13 V (DCEN), and the travel speed was 3.3 mm $s^{-1}$. During the weld, once steady state was established, a jet of water was directed on the weld pool effectively decanting the liquid metal and quenching the surrounding metal. The area surrounding the quenched region was sectioned out and prepared for metallographic examination.

Differential thermal analysis (DTA) work was also performed to determine a temperature used to calculate the $M_{dc}$ using Eq. (3) for each alloy. To run the DTA each alloy was heated in the as-cast condition to above its melting point at a rate of 20 °C $min^{-1}$. A typical heating curve is shown in Fig. 1. The smaller secondary peaks indicate the melting of secondary phases while

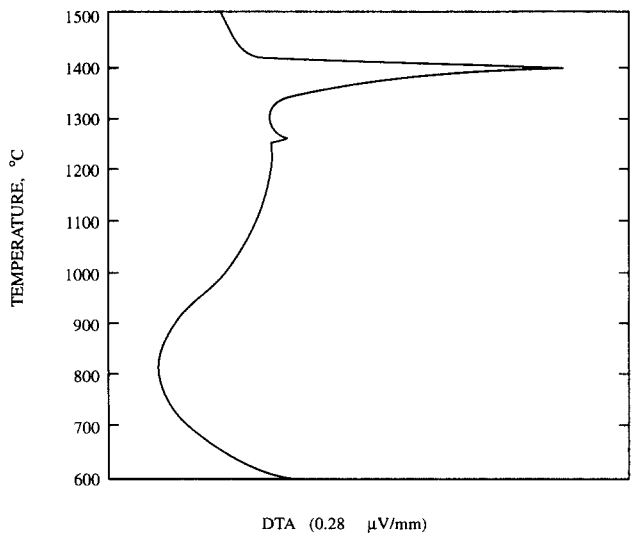


Fig. 1. DTA profile on heating Alloy 1. Secondary peaks indicate the melting of minor solidification constituents.

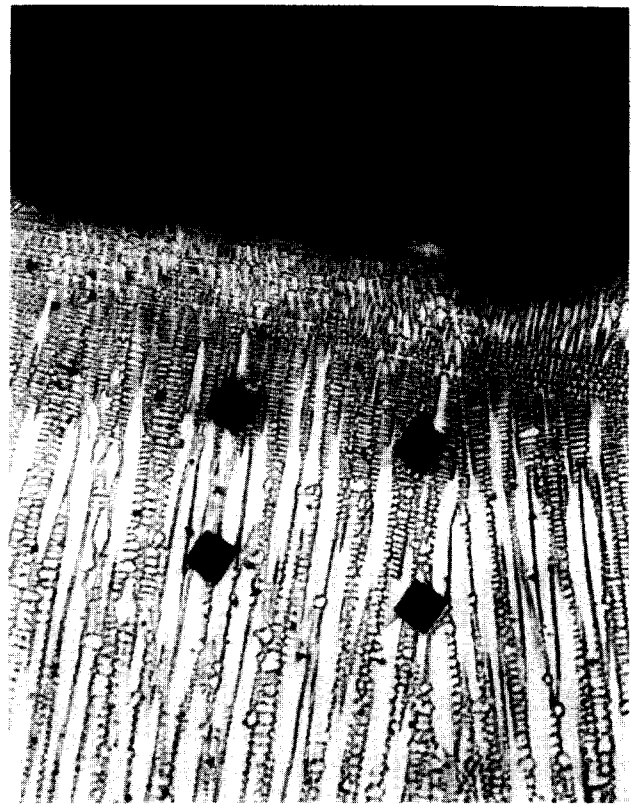

Fig. 2. Light micrograph of area near quenched region in weld metal to be analyzed.

the large peak corresponds to the melting of the bulk alloy.

## 3. Results and discussion

The area suitable to be analyzed is in the region of parallel growing dendrites near the quenched zone (Fig. 2). The microhardness impressions shown in this figure were used to identify the selected area when using a scanning electron microscope (SEM). To quantify the amount of segregation, energy dispersive spectra (EDS) were taken in one or two micron increments across several dendrites in all weld metal specimens. The results of these composition scans for an alloy representative of each series with corresponding $M_d$ levels calculated according to Eq. (2) are shown in Figs. 3 and 4.

Alloys 1–4 are the series of four molybdenum containing alloys, which are of an alloy system that can involve sigma-type phases. As these weld metals solidify, molybdenum segregates to the interdendritic regions. A representative composition profile with corresponding $M_d$ level profiles showing this segregation is given in Fig. 3. In this series, the critical value for formation of the sigma phase was exceeded in the weld metal of each alloy. This behaviour can be seen in

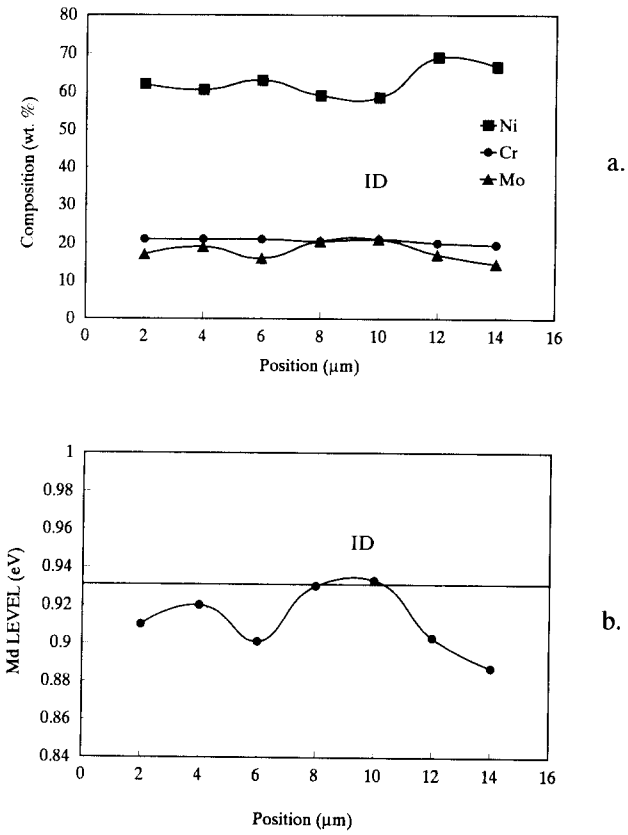


Fig. 3. (a) Composition profile of weld metal in Alloy 1; (b) corresponding metal-d level, $M_d$, profile of Alloy 1 showing placement of critical value.

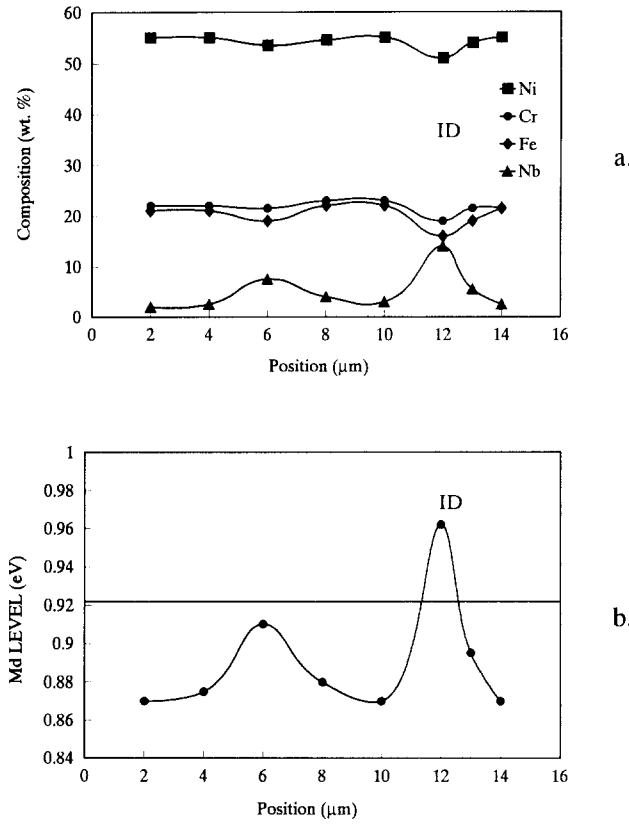


Fig. 4. (a) Composition profile of weld metal in Alloy 5; (b) corresponding metal-d level, $M_d$, profile of Alloy 5 showing placement of critical value.

Table 2 where the difference between maximum $M_d$ and critical $M_d$ is positive. The presence of secondary phases was confirmed with the DTA. As expected, the maximum $M_d$ obtained in the interdendritic region increases with the bulk $M_d$ as does the fraction of TCP due to the increasing amount of molybdenum. It is interesting that homogenized wrought alloys of these compositions are predicted to be unable to form a TCP phase as seen by the negative differences between the bulk $M_d$ and the critical $M_d$ values.

To compare the results of the segregation profiles of Series I alloy weld metals and the validity of the New PHACOMP calculations applied to these profiles, the equivalent segregation patterns were plotted on a Ni–Cr–Mo phase diagram. Fig. 5 is the nickel-rich portion of the Ni–Cr–Mo phase diagram at 1250 °C with equivalent composition profiles plotted for Alloys 1–4. The equivalent compositions were determined using Eqs. (4), (5), and (6), as developed by Cieslak et al. [12].

$$\mathrm{Mo(eq)} = \mathrm{Mo} + \mathrm{W} \quad (4)$$

$$\mathrm{Cr(eq)} = \mathrm{Cr} \quad (5)$$

$$\mathrm{Ni(eq)} = \mathrm{Ni} + \mathrm{Fe} + \mathrm{X} \quad (6)$$

Table 2
Bulk $M_d$, critical $M_d$ and maximum $M_d$ calculated for Alloys 1–8. The critical $M_d$, $M_{dc}$, was calculated using Eq. 3 with the temperature determined by DTA. The difference between the bulk $M_d$ and the critical $M_d$ and the difference between the maximum $M_d$ and the critical $M_d$ are also listed. If a difference is positive, it would suggest that the TCP phase could possibly form

| Alloy | Bulk $M_d$ | Crit. $M_d$ | Bulk $M_d$-Crit. $M_d$ | Max. $M_d$ | Max. $M_d$ – Crit. $M_d$ |
|---|---|---|---|---|---|
| 1 | 0.90 | 0.929 | −0.01 | 0.93 | +0.001 |
| 2 | 0.91 | 0.930 | −0.02 | 0.95 | +0.02 |
| 3 | 0.90 | 0.930 | −0.03 | 0.97 | +0.04 |
| 4 | 0.93 | 0.930 | 0.00 | 0.96 | +0.03 |
| 5 | 0.90 | 0.922 | −0.02 | 0.96 | +0.04 |
| 6 | 0.90 | 0.924 | −0.02 | 0.95 | +0.03 |
| 7 | 0.86 | 0.925 | −0.06 | 0.92 | −0.005 |
| 8 | 0.83 | 0.926 | −0.10 | 0.89 | −0.04 |

The critical $M_d$ line at 1250 °C is also plotted and is shown as the dashed line. In Fig. 5, the critical $M_d$ line does a good job of predicting the boundary between gamma phase and the TCP phases; P and sigma phases. The equivalent bulk compositions of Alloys 1–4 are plotted as the four points. The arrows indicate an equivalent composition profile of each alloy starting at the dendrite core and traversing towards the interdendritic region. The bulk equivalent compositions as well as the dendrite cores of these alloys are in the single-phase gamma region while the interdendritic regions all cross the critical $M_d$ line towards the gamma + P and gamma + sigma phase regions. These results are an excellent example of the ability of New PHACOMP calculations to predict sigma phase formation.

Each series II alloy was designed with a different tendency to form Laves phase as characterized by the bulk $M_d$ level. As these alloys solidify, the dendrite core is enriched in nickel, chromium, and iron while partitioning niobium to the interdendritic region. This typical behaviour can be seen in Fig. 4(a). The segregation pattern results in an increase in the $M_d$ level shown in the corresponding Fig. 4(b). The average $M_d$ exceeds the critical $M_d$ in the interdendritic region of Alloys 5 and 6. The $M_d$ level in Alloys 7 and 8 does not rise above the critical value. Fig. 6 shows this behaviour. Even though the $M_d$ value remained below the critical value, DTA indicated the presence of secondary phases. The secondary phases expected to form in this series are Laves and possibly $Ni_3Nb$. The morphology of secondary phase found in Alloy 8 weld metal is very similar to Laves phase as identified by Cieslak (12) in Inconel 625 weld metal.

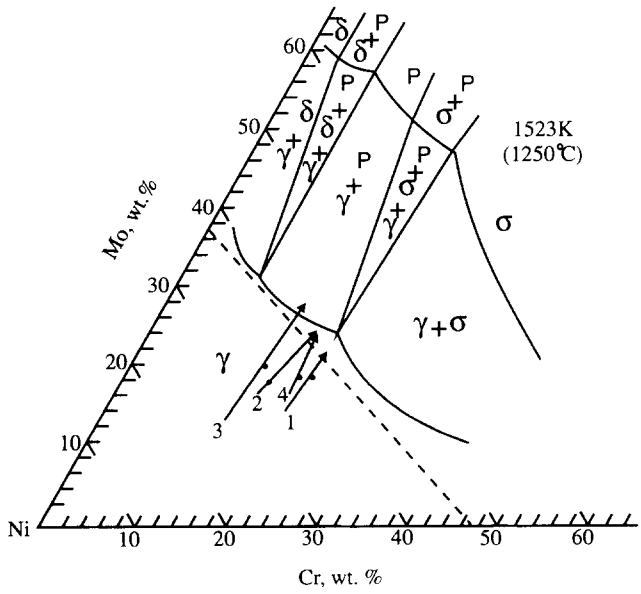


Fig. 5. Nickel-rich portions of Ni–Cr–Mo ternary phase diagram at 1250 °C showing placement of the critical New PHACOMP line (dashed line) and equivalent solidification profiles of Alloys 1–4 as arrows.

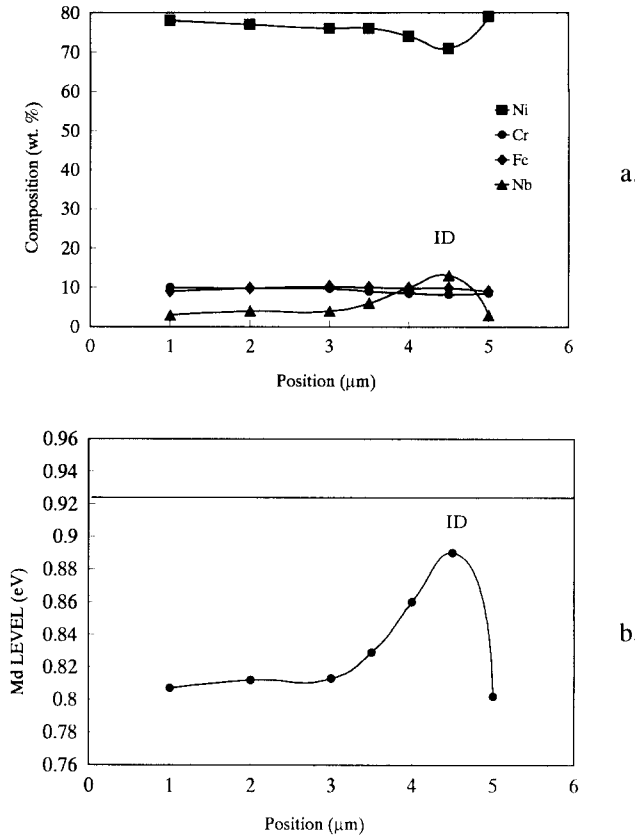


Fig. 6. (a) Composition profile of weld metal in Alloy 8; (b) corresponding metal-d level, $M_d$, profile of Alloy 8 showing placement of critical value.

For series II alloys the maximum $M_d$ obtained in the interdendritic region is related to the bulk $M_d$. As the bulk $M_d$ level increases, the maximum Md obtained in the interdendritic also increases. These results are shown in Table 2. Secondary phases were found to form in all series II weld metal specimens. The fraction of secondary phases present was observed to increase with the bulk $M_d$. This effect is a result of the increasing niobium content. Homogeneous wrought alloys of these compositions are predicted to be unable to form a TCP phase as seen by the negative difference between the bulk $M_d$ and the critical $M_d$ values. The calculations also predicted that weld metal of alloy 5 and 6 should be able to form TCP phases as seen by the positive difference between the maximum $M_d$ and critical $M_d$ values. It also predicted that weld metal of alloys 7 and 8 should not form TCP phases.

The presence of a Laves-type phase in Alloy 8, in which the critical $M_d$ is not exceeded, suggests that the matrix is reaching a critical $M_d$ value lower than that predicted by the temperature-dependent critical $M_d$ equation. This result supports the assertion of Morinaga et al. [22] where it is suggested that the critical value for formation of the Laves phase (a size-effect intermetallic compound) may be lower than that for

sigma phase. This observation also implies that the temperature-dependent critical $M_d$ equation (Eq. (3)) cannot be simply extended to include the formation of Laves-type phases. Comparing the compositional and $M_d$ profiles results shown in Table 2 suggests that the critical $M_d$ for Alloys 5–8 may be less than 0.89. It becomes apparent that specific temperature-dependent critical $M_d$ equations need to be determined for each type of TCP phase.

## 4. Conclusions

1. An evaluation of New PHACOMP analysis for predicting the susceptibility of nickel alloy weld metal to form topologically close-packed phases was performed.

2. The formation of sigma-type phases correlated well with the critical $M_d$ level calculations as defined by New PHACOMP.

3. The formation of Laves phase, a size-effect intermetallic compound, did not correlate well with the critical $M_d$ level calculations as defined by New PHACOMP for the formation of sigma-phase-type phases.

## Acknowledgement

This work was performed with support by Sandia National Laboratories which is supported by the US Department of Energy under contract number DE-AC04-94AL-85000.

## References

[1] F.J. Hodge, Effect of aging on the anodic behaviour of Ni–Cr–Mo alloys, *Corrosion*, *29*(10) (1973) 375–383.
[2] E.A. Loria, The status and prospects of alloy 718, *J. Metals*, *40*(7) (1988) 36–41.
[3] M.J. Cieslak, A.D. Romig Jr., and T.J. Headly, Weld metal hot cracking of Hastelloy alloys C-22 and C-276: A study by analytical electron microscopy, in J.T. Armstrong (ed.), *Microbeam Analysis*, San Francisco Press, CA, 1985, pp. 179–188.
[4] R.G. Thompson, Microfissuring of Alloy 718 in the weld heat-affected zone, *J. Metals*, *40*(7) (1988) 44–48.
[5] C.T. Sims, A contemporary view of nickel-base superalloys, *J. Metals*, *18*(10) (1966) 1119–1130.
[6] E.W. Ross, Rene 100: a sigma free turbine blade alloy, *J. Metals*, *19*(12) (1967) 12–14.
[7] R.B. Leonard, Thermal stability of Hastelloy alloy c-276, *Corrosion*, *25*(5) (1967) 222–228.
[8] M. Raghavan, B.J. Berkowitz and J.C. Sanlon, Electron microscopic analysis of heterogeneous precipitates in Hastelloy C-276, *Met. Trans.*, *13A*(6) (1982) 979–984.
[9] M.J. Cieslak, J.J. Stephens and M.J. Carr, A study of the related microstructures of Cabot alloy 214, *Met. Trans.*, *19A*(3) (1988) 657–667.
[10] M.J. Cieslak, A.M. Ritter and W.F. Savage, Solidification cracking and analytical electron microscopy of austenite stainless steel weld metal, *Welding J.*, *61*(1) (1982) 1s–8s.
[11] M.J. Cieslak, A.M. Ritter and W.F. Savage, Chi-phase formation during solidification and cooling of cf-8M weld metal, *Welding J.*, *63*(4) (1984) 133s–140s.
[12] M.J. Cieslak, T.J. Headley and A.D. Romig Jr., The welding metallurgy of Hastelloy alloys C-4, C-22 and C-276, *Met. Trans.*, *17A*(11) (1986) 2035–2047.
[13] C.T. Sims and W.C. Hagel, *The Superalloys*, Wiley, New York, 1972.
[14] M. Raghavan, R.R. Mueller, G.A. Vaughn and S. Floreen, Determination of isothermal sections of nickel rich portion of Ni–Cr–Mo systems by analytical electron microscopy, *Met. Trans.*, *15A*(5) (1984) 783–792.
[15] D.K. Das, S.P. Rideout and P.A. Beck, Intermediate phases in the Mo–Fe–Co, Mo–Fe–Ni and Mo–Ni–Co ternary systems, *Trans. TMS-AIME*, *194* (1952) 1071–1075.
[16] L. Pauling, The nature of the interatomic forces in metals, *Phys. Rev.*, *54* (1938) 899–904.
[17] P. Greenfield and P. Beck, The sigma phase in binary alloys, *Trans. TMS-AIME*, *200* (1953) 253–257.
[18] P. Greenfield and P. Beck, Intermediate phases in binary systems of certain transition elements, *Trans.TMS-AIME*, *206* (1956) 265–276.
[19] L.R. Woodyatt, C.T. Sims and H.J.Beattie, Prediction of sigma-type phase occurrence from compositions in austenitic superalloys, *Trans. TMS-AIME*, *236*(4) (1968) 518–527.
[20] H.J. Murphy, C.T. Sims and A.M. Beltran, PHACOMP revisited, *J. Metals*, *20*(11) (1968) 46–53.
[21] R.J. Barrows and J.B. Newkirk, Modified system for predicting sigma formation, *Met. Trans.*, *3*(11) (1972) 2889–2893.
[22] M. Morinaga, N. Yukawa, H. Adachi and H. Ezaki, New PHACOMP and its application to alloy design, *Superalloys 1984*, TMS, Philadelphia, 1984, pp. 523–532.
[23] M. Morinaga, N. Yukawa, H. Adachi and H. Ezaki, Alloying effect on the electronic structure of $Ni_3Al$, *J. Phys. Soc. Jpn.*, *53*(2) (1984) 653–663.
[24] M.J. Cieslak, G.A. Knorovsky, T.J. Headley and A.D. Romig, Jr., The use of New PHACOMP in understanding the solidification microstructure of nickel base alloy weld metal, *Met. Trans.*, *17A*(12) (1986) 2107–2115.